BIOCHEMISTRY
including biophysical chemistry & molecular biology
Article

Biochemistry **2010,** *49,* 10187–10197 10187
DOI: 10.1021/bi1015056

Kinetic Stability May Determine the Interaction Dynamics of the Bifunctional Protein DCoH1, the Dimerization Cofactor of the Transcription Factor HNF-1α[†,‡]

H. Rho, C. N. Jones,[§] and R. B. Rose*

Department of Molecular and Structural Biochemistry, 128 Polk Hall, North Carolina State University, Raleigh, North Carolina 27695, United States. [§]*Current address: College of Science and Technology, 1209 Mary M. Townes Science Complex, North Carolina Central University, Durham, NC 27707*

Received September 16, 2010; Revised Manuscript Received October 23, 2010

ABSTRACT: The two disparate functions of DCoH1 (dimerization cofactor of HNF-1)/PCD (pterin-4a-carbinolamine dehydratase) are associated with a change in oligomeric state. DCoH dimers enhance the activity of the diabetes-associated transcription factor HNF-1α (hepatocyte nuclear factor-1α), while the PCD activity of DCoH1 homotetramers aids in aromatic amino acid metabolism. These complexes compete for the same interface of the DCoH dimer. Formation of the DCoH1/HNF-1α complex requires cofolding. The homotetramer of the DCoH1 paralogue, DCoH2, interacts with HNF-1α through simple mixing. To further investigate regulation of DCoH/HNF-1α complex formation, we measured the stability of the DCoH1 homotetramer through unfolding studies by intrinsic tryptophan fluorescence. DCoH2 unfolding is reversible. Surprisingly, the DCoH1 homotetramer is resistant to guanidine unfolding but refolds at a much lower guanidine concentration. We show that a point mutation at the DCoH1 tetramer interface, Thr 51 Ser, overcomes the dissociation barrier of the homotetramer and increases the interaction with HNF-1α. The 1.8 Å resolution crystal structure of DCoH1 T51S shows the presence of an ordered water molecule at the tetramer interface, as in DCoH2, which may destabilize the homotetramer. The equilibrium unfolding data were fit to a two-state model with no apparent intermediate. Folding intermediates were detectable by size exclusion chromatography. For wild-type DCoH1 the intermediates changed with time, suggesting a kinetic origin for the unfolding barrier of the homotetramer. We propose an unfolding pathway in which the tetramer unfolds slowly, but the dimer folds reversibly. Implications for regulation of DCoH1/HNF-1α complex formation are discussed.

Transcriptional coactivators frequently fulfill multiple regulatory roles by binding different protein partners. This is true of general coactivators, such as CBP and p300, which can interact with many different transcription factors (*1*, *2*). It is also true of more specialized coactivators, such as DCoH,[1] OcaB, and SRC, which regulate specific transcription factors (*3*, *4*). A number of specialized coactivators have been shown to be bifunctional, fulfilling nontranscriptional roles through interactions with other proteins (*5*). The molecular basis for selection among partners is important for determining how these coactivators regulate transcription.

The bifunctional protein DCoH (dimerization cofactor of HNF-1) provides an example of a multipurpose interface that mediates distinct protein−protein interactions (*6*−*9*). In the cytoplasm, DCoH, also called pterin-4a-carbinolamine dehydratase (PCD), functions as a metabolic enzyme (*10*, *11*). The PCD activity regenerates tetrahydrobiopterin, a cofactor of nitric oxide synthase and aromatic amino acid hydroxylases (*12*, *13*). Mutations in DCoH1 cause transient hyperphenylalaninemia (*14*−*16*). In the nucleus, DCoH functions as a coactivator to enhance the transcriptional activity of HNF-1α or HNF-1*β*, in part by stabilizing HNF-1 dimers (*3*). In both contexts, DCoH folds into a tetrameric structure. As a metabolic enzyme it forms a homotetramer (a dimer of dimers). As a coactivator a dimer of DCoH interacts with a dimer of HNF-1 (*7*, *9*). Both complexes compete for the same tetramerization interface of the DCoH dimer (Figure 1).

DCoH1 carries out its diverse functions in different cellular contexts. DCoH1 functions as an enzyme and a coactivator in liver, kidney, small intestine, and pancreas, tissues that also express HNF-1 (*3*, *17*, *18*). Consistent with its independent enzymatic function, DCoH1 is also expressed in skin, brain, heart, and eye. DCoH1 may also interact with nuclear factors other than HNF-1 (*17*, *19*, *20*). The importance of HNF-1α and HNF-1*β* in pancreatic *β* cells was demonstrated by inherited mutations associated with maturity-onset diabetes of the young type 3 (MODY3) (*21*) and type 5 (MODY5) (*22*), respectively. DCoH1 levels in the liver have been estimated at about 4−6 *μ*M (*11*, *23*, *24*), while HNF-1α is present at low nanomolar concentrations (*15*, *25*, *26*). We are not aware of concentration measurements in pancreatic *β* cells. A paralogue of DCoH1, DCoH2

[†]This work was supported by the National Science Foundation under Grant MCB-0643830. Use of the Advanced Photon Source was supported by the U.S. Department of Energy, Office of Science, Office of Basic Energy Sciences, under Contract W-31-109-Eng-38.

[‡]Coordinates and structure factors have been deposited in the Protein Data Bank with the accession code 1HXA.

*To whom correspondence should be addressed. Phone: (919) 513-4191. Fax: (919) 515-2047. E-mail: bob_rose@ncsu.edu.

[1]Abbreviations: DCoH, dimerization cofactor of HNF-1; DTT, dithiothreitol; GST, glutathione *S*-transferase; GdnHCl, guanidinium chloride; HNF-1, hepatocyte nuclear factor-1; MWCO, molecular weight cutoff; PBS, phosphate-buffered saline; PCD, pterin-4a-carbinolamine dehydratase; SDS−PAGE, sodium dodecyl sulfate−polyacrylamide gel electrophoresis; SEC, size exclusion chromatography; wt, wild type; *β*-ME, *β*-mercaptoethanol; ΔASA, change in solvent-accessible surface area.

Published on Web 10/25/2010

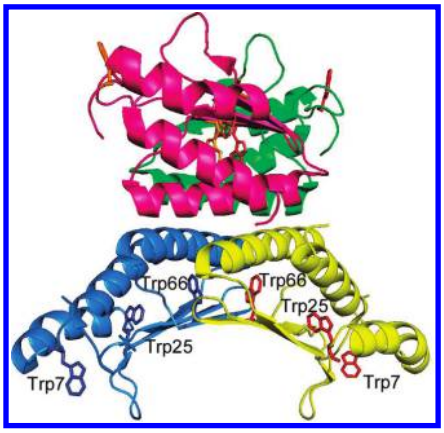

FIGURE 1: Ribbon diagram representation of the tetrameric DCoH2 showing the positions of the tryptophans. The magenta/green and blue/yellow pairs each represent a DCoH2 dimer. The three tryptophan side chains, at positions 7, 25, and 66, are shown as stick representations. DCoH1 (not shown) has only two tryptophans at positions 25 and 66. The structure was generated with PyMol using PDB id 1RU0.

(or DCoHm), retains the same enzymatic and coactivator functions as DCoH1 and is also expressed in liver, kidney, and intestine (*17*, *27*). Human DCoH1 and DCoH2 share 61% sequence identity. Unlike DCoH1, DCoH2 is highly expressed in muscle, and DCoH1 and DCoH2 are reportedly expressed in different phases of the cell cycle (*28*).

Characterizations of the properties of DCoH1 governing formation of the DCoH1/HNF-1α coactivator complex have centered on the hyperstability of the DCoH1 homotetramer *in vitro* (*9*, *15*, *29*). The DCoH1 homotetramer is thermally stable when heated to 90 °C (*29*). Consistent with the stability of the homotetramer, DCoH1 fails to interact with the HNF-1α dimerization domain if mixed *in vitro* (*9*, *29*−*31*). The DCoH/HNF-1α complex forms by coexpression of DCoH1 and HNF-1α or after denaturing DCoH1 in guanidinium chloride (GdnHCl) and renaturing in the presence of the HNF-1α dimerization peptide (*9*, *29*−*31*). These observations led to the idea that the DCoH1 homotetramer is thermodynamically very stable, while the DCoH/HNF-1α complex is kinetically formed and trapped (*32*). There is no evidence to date for chaperone-mediated folding of DCoH. In contrast, the DCoH2 homotetramer purportedly dissociates into dimers in solution (*15*, *32*). A DCoH2/HNF-1α complex can form by mixing the DCoH2 homotetramer and HNF-1α *in vitro*, suggesting that the DCoH2 homotetramer is less stable than the DCoH1 homotetramer.

In order to further investigate the relative stabilities of the DCoH1 and DCoH2 homotetramers, we performed chemical denaturation studies using GdnHCl. Equilibrium unfolding of DCoH2 was fit to a two-state model. Surprisingly, the DCoH1 homotetramer is resistant to guanidine unfolding, with unfolding intermediates changing over time. This suggests that the DCoH1 homotetramer is not thermodynamically hyperstable as previously thought but is very slow to unfold or kinetically stable (*33*). A point mutant in the tetramer interface, Thr 51 Ser, decreases the homotetramer stability so it unfolds reversibly. Kinetic stability of the DCoH1 homotetramer has implications for formation of the complex with HNF-1 *in vivo*.

EXPERIMENTAL PROCEDURES

DCoH Purification. Mouse DCoH2 (*32*) and rat DCoH1 (*7*) subcloned into the pGEX-2T vector (Pharmacia) were overexpressed in *Escherichia coli* strain BL21 (Novagen) as fusion proteins with glutathione *S*-transferase. To generate the DCoH1 T51S mutation, the ACA codon for Thr 51 was substituted with the TCA codon for Ser using the primer C AGG GCT TTT GGC TTC ATG TCA AGA GTC GCC CTG CA (the mutated codon is underlined) by PCR-based mutagenesis in the rat DCoH1 pGEX-2T vector (*34*). Cells were grown at 37 °C to OD 0.6, induced overnight at 22 °C with 1 mM isopropyl β-D-1-thiogalactopyranoside (IPTG), lysed in 50 mM Tris (pH 8.5), 300 mM NaCl, and 1 mM dithiothreitol (DTT), and purified with glutathione Sepharose 4 Fast Flow resin (Amersham Pharmacia) according to the manufacturer's instructions. The GST tag was removed by thrombin cleavage for 5 h at room temperature, as described by the manufacturer (MPBio). Thrombin was subsequently removed on a *p*-aminobenzamidine agarose column (Sigma). Protein was concentrated with an Amicon Ultra centrifugal filter device (5K MWCO; Millipore). The final purified proteins were greater than 95% pure as judged from a Coomassie Blue-stained (Sigma) SDS−PAGE NEXT gel (ISC BioExpress) (data not shown). Protein concentrations were measured by Bradford (Bio-Rad) for DCoH1 and DCoH1 T51S using albumin as a standard and UV absorbance for DCoH2 in 8 M GdnHCl with the calculated extinction coefficient ε = 19480 M^{-1} cm^{-1} (*35*, *36*).

Affinity Chromatography Assay. Mouse HNF-1α (residues 1−280) with a C-terminal His_6 tag (HNF-1α 1−280-His_6) subcloned into the pET24b vector (Novagen) (*32*) was expressed in *E. coli* strain BL21 (DE3) (Novagen). Cells were grown at 37 °C to 0.6 OD and induced overnight at 22 °C with 1 mM IPTG. Cells were sonicated in PBS (pH 7.4), 10 mM imidazole, and 20 mM β-mercaptoethanol (β-ME) and purified on a His-Select nickel column (Sigma) according to the manufacturer's instructions. HNF-1α 1−280-His_6 was eluted from the column with an imidazole gradient (20−250 mM imidazole) and treated with 0.2% polyethylenimine (PEI; Sigma) for 20 min at 4 °C to remove DNA. The final protein was concentrated and buffer exchanged into 50 mM Tris (pH 8.0), 300 mM NaCl, and 20 mM β-ME using an Amicon Ultra centrifugal filter device (10K MWCO; Millipore). The final purified protein was greater than 95% pure as judged from a Coomassie-stained SDS−PAGE gel (data not shown).

Interaction between HNF-1α and DCoH was measured with HNF-1α 1−280-His_6 immobilized on Ni^{2+}-chelating resin (Qiagen) as described with minor modifications (*32*). Briefly, 40 μg of HNF-1α was bound to 20 μL of resin preequilibrated in PBS (pH 7.4), 30 mM imidazole, and 20 mM β-ME buffer. The resin was washed extensively and incubated with purified DCoH1, DCoH1 T51S, or DCoH2 (40 μg). Resin was washed twice with 550 μL of buffer and 3 times with 200 μL of buffer. Sample loading buffer was added to the resin and analyzed with a 12.5% SDS−PAGE NEXT gel (ISC BioExpress) stained with Coomassie Blue (Sigma).

DCoH1 T51S Structure Determination. DCoH1 T51S (13 mg/mL) crystallized with Hampton Crystal Screen no. 39 (0.1 M HEPES-Na, pH 7.5, 2% (v/v) PEG400, 2.0 M ammonium sulfate), similar to the conditions for crystallization of wild-type DCoH1 (*7*). Crystals were briefly soaked in a cryoprotectant composed of 0.1 M HEPES-Na (pH 7.5), 2.0 M ammonium sulfate, 4% (v/v) PEG200, and 22.5% glycerol and flash frozen in liquid nitrogen. Data were collected to 1.8 Å at the Southeast Regional Collaborative Access Team (SER-CAT) beamline 22-ID at the Advanced Photon Source (Argonne, IL). The data were indexed in space group $P3_221$ with MOSFLM (*37*) and

Table 1: Data Collection and Refinement Statistics

	DCoH1 T51S
data collection	
space group	$P3_221$
cell dimensions	
a, *b*, *c* (Å)	103.8, 103.8, 193.6
α, *β*, *γ* (deg)	90.00, 90.00, 120.00
resolution (Å)	50−1.8 (1.9−1.8)[a]
R_{sym} or R_{merge}	0.118 (0.921)
$I/\sigma I$	3.0 (0.8)
Mn(I)/sd	12.2 (2.5)
completeness (%)	99.1 (96.6)
redundancy	9.7 (8.2)
refinement	
resolution (Å)	1.8
no. of reflections	111045
R_{work}/R_{free}	21.05/22.57
no. of atoms	
protein	6445
ligand/ion	88
water	524
B-factors	
protein	30.80
ligand/ion	50.88
water	44.51
rms deviations	
bond lengths (Å)	0.006
bond angles (deg)	1.198

[a]Values in parentheses are for the highest resolution shell.

scaled with Scala, and *F*'s were calculated with Truncate using the ELVES interface (Table 1) (*38*−*41*). The space group and unit cell dimensions indicated the packing of DCoH1 T51S in the crystal was the same as for PDB id 1DCH (*7*). An initial model consisting of two DCoH1 homotetramers, with Thr 51 changed to Ala and with water molecules removed, was positioned relative to the DCoH1 T51S crystal data by rigid body refinement with CNS, allowing the position of each homotetramer to refine independently, resulting in an *R*-factor of 50.5% (*42*). After positional refinement and *B*-factor refinement, the *R*-factor and *R*-free dropped to 32% and 35%, respectively. The model was further refined with CNS alternated with manual building using the programs O (*43*) and Coot (*44*). The final 1.8 Å resolution model (see Table 1 for refinement statistics) includes 397 amino acids for one tetramer (chains A−D), 399 amino acids for the second tetramer (chains E−H), 524 water molecules, 1 sulfate molecule per protein monomer, and 4 glycerol molecules associated with each tetramer.

Structure figures were generated with Pymol (*45*). The cavity at the tetramer interface was calculated with the program Voidoo (*46*) and written out in ezd format. The cavity was displayed in Pymol after being converted to Xplor format using Mapman (*47*).

Fluorescence Unfolding Studies. DCoH unfolding was monitored by guanidinium chloride (GdnHCl; Pierce) induced denaturation by intrinsic tryptophan fluorescence using a PTI C-61 spectrofluorometer (Photon Technology International). DCoH1 monomers contain two Trp residues, and DCoH2 monomers contain three Trp residues. Only one tyrosine is present in both DCoH1 and DCoH2. Excitation at 280 and 295 nm produced the same emission profiles, indicating the fluorescence signal is dominated by the tryptophans (not shown). Fluorescence measurements were acquired at 25 °C using an excitation wavelength of 280 nm and emission scans from 300 to 400 nm. The scan rate was 1 nm/s. Emission data at 330 nm were used for the folding profiles.

For folding studies, all experiments were carried out at pH 7.4 in phosphate buffer. Concentrated DCoH stocks were diluted into phosphate buffer, pH 7.4, containing 50 mM KH_2PO_4/K_2HPO_4 (Sigma, J.T. Baker), 1 mM DTT (Sigma), plus or minus GdnHCl. The GdnHCl concentration was checked by refractive index with a Fischer Scientific refractometer using the equation described in ref *48*. Solutions were prepared fresh for each experiment and filtered through 0.22 *μ*m pore sized filters (Whatman Puradisc). Unfolding reactions were carried out in 2 mL low retention tubes (Sigma) to minimize protein loss.

Unfolding and refolding curves were compared to confirm that protein samples had reached equilibrium. For unfolding experiments, concentrated protein stocks were diluted with phosphate buffer containing 0−4 M GdnHCl. For refolding experiments, concentrated protein stocks were unfolded in phosphate buffer containing 4 M GdnHCl and incubated overnight. The fluorescence emission profiles at 4 and 6 M GdnHCl were identical (not shown); therefore, 4 M GdnHCl was used for unfolding. The following day, samples were diluted to the appropriate denaturant and protein concentrations with phosphate buffer and phosphate buffer containing GdnHCl. All samples were incubated overnight prior to measurement unless otherwise indicated. Equilibrium unfolding experiments for DCoH1 T51S were carried out by premixing two protein stock solutions having the same final protein concentration: one in phosphate buffer and a second in phosphate buffer containing 4 M GdnHCl. Various volumes of the 0 and 4 M GdnHCl protein solutions were mixed to the appropriate GdnHCl concentrations and incubated overnight prior to measurement. Under equilibrium conditions, emission spectra were measured at 0.5, 1.05, 2.1, and 4.2 *μ*M protein concentrations. All protein concentrations are reported in terms of DCoH monomers. For DCoH2, unfolding and refolding data were compared to obtain the final equilibrium curve.

Fluorescence emission data were analyzed by first subtracting the buffer background at the appropriate GdnHCl concentration, which was interpolated from the emission signal measurements of phosphate buffer and phosphate buffer containing 4 M GdnHCl. Fluorescence data were normalized using the equation:

$$I = \frac{(Y - Y_U)}{(Y_N - Y_U)}$$

in which *I* is the normalized signal (typically ranging from 0 to 1), *Y* the signal at a given GdnHCl concentration, Y_N the signal in phosphate buffer, and Y_U the signal in phosphate buffer containing 4 M GdnHCl.

Modeling. The normalized unfolding signal was monophasic. The data were fit to the two most likely two-state models: from dimer to monomer ($N_2 \leftrightarrow 2U$), as described in ref *49* and from tetramer to monomer ($N_4 \leftrightarrow 4U$) (Supporting Information Figure S1, as described in ref *50*). The model includes linear baselines for low and high GdnHCl concentrations. The quartic equation has single real solutions, according to Descartes' rule of signs. Data were fit using the program Igor Pro (WaveMetrics, Inc.). The Igor Pro algorithms used to fit the data are included as Supporting Information (Figure S2). The *m*-value and ΔG_{H_2O} were fit globally to the equilibrium unfolding data, with local baseline corrections fit to each protein concentration (Supporting Information Figure S3). Solvent-accessible surface areas (*51*) were calculated by NACCESS (*52*).

Size Exclusion Chromatography. Size exclusion chromatography (SEC) analysis was carried out on a TSK-GEL Super SW2000 column (Tosoh) and a Biosep-SEC-S3000 column (Phenomenex). The dimensions of both columns were 300 mm × 4.6 mm. Mobile phase flow was controlled by a Waters 1525 binary HPLC pump. The columns were preequilibrated in 50 mM KH_2PO_4/K_2HPO_4, pH 7.4, plus GdnHCl at the same concentration as the sample, at a flow rate of 0.35 mL/min at room temperature. Ten microliters of sample was injected with an autosampler (Waters, 717 Plus). Elution profiles were detected at 220 and 280 nm with a UV absorbance detector (Waters, 2487). Unfolding and refolding samples were prepared as described for fluorescence unfolding studies. The samples contained 2.1 μM DCoH, 50 mM KH_2PO_4/K_2HPO_4 1 mM DTT, and different concentrations of GdnHCl, unless otherwise specified. In order to normalize for the salt effect at different GdnHCl concentrations, the chromatograms were translated so the DTT peak overlapped with the DTT peak at low GdnHCl concentration. A calibration curve was plotted for each column using gel filtration standards (Bio-Rad catalog number v151−1901) eluted with 0.05 M Na_2HPO_4, 0.05 M NaH_2PO_4, and 0.15 M NaCl, pH 6.8. The elution volumes, V_e, were fit to a linear function of log of the molecular weight.

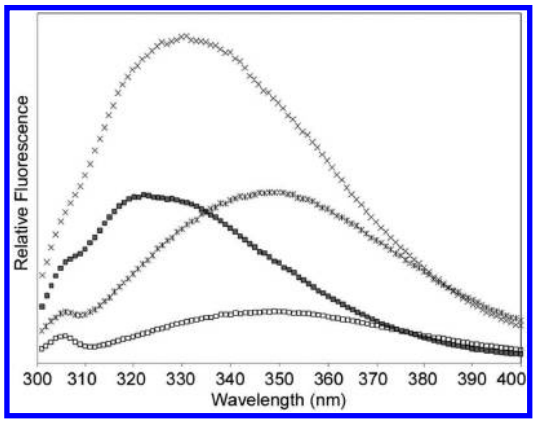

FIGURE 2: Relative fluorescence emission spectra of native and denatured DCoH2 and DCoH1 at 2.1 μM protein in phosphate buffer containing 0 or 4 M GdnHCl. The proteins were denatured with 4 M GdnHCl and incubated overnight. DCoH2 denaturation resulted in a red shift of λ_{max} from 333 nm at 0 M GdnHCl (×) to 356 nm at 4 M GdnHCl (*). Denaturation of DCoH1 resulted in a red shift of λ_{max} from 322 nm at 0 M GdnHCl (■) to 356 nm at 4 M GdnHCl (□). The emission signal is displayed on an arbitrary scale for comparison. The overall emission signal for DCoH2 is greater than for DCoH1 due to the additional Trp residue per monomer. The excitation wavelength was 280 nm.

RESULTS

DCoH Unfolding Monitored by Intrinsic Tryptophan Fluorescence. Unfolding of DCoH1 and DCoH2 was monitored by the intensity change of the intrinsic tryptophan fluorescence. The DCoH1 monomer contains two tryptophans at positions 25 and 66 (Figure 1). DCoH2 contains the same two tryptophans as DCoH1 as well as a third tryptophan at position 7.

DCoH1 is thermally stable (*29*). Therefore, chemical denaturation was used to unfold the proteins. Surprisingly, DCoH1 was resistant to denaturation in 8 M urea (not shown) but did unfold in GdnHCl (Figure 2). DCoH1 and DCoH2 were completely unfolded after incubating overnight in 4 M GdnHCl.

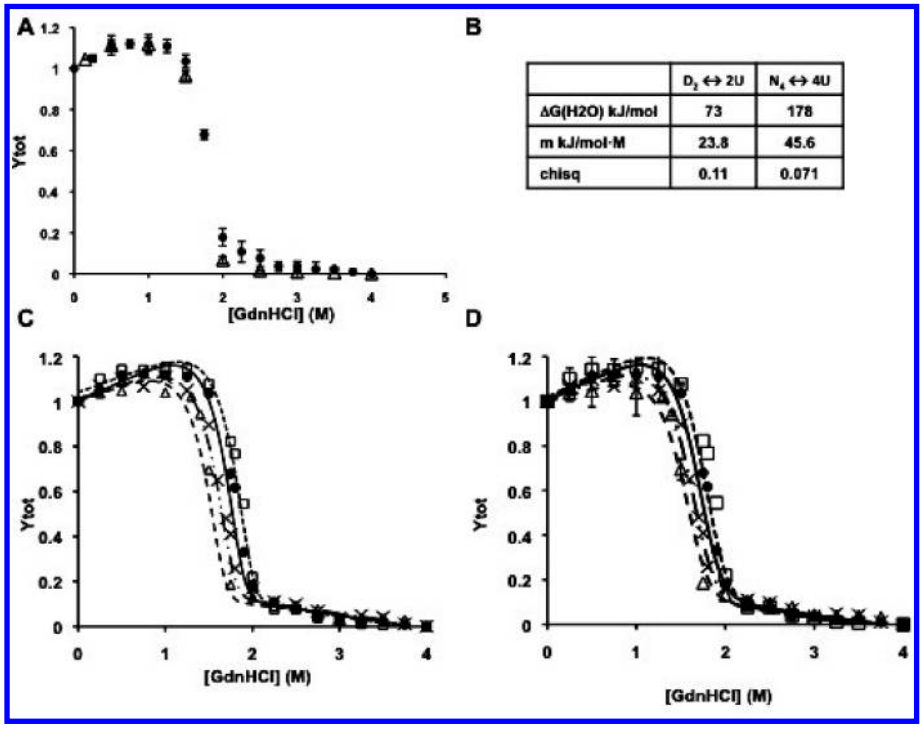

	$D_2 \leftrightarrow 2U$	$N_4 \leftrightarrow 4U$
ΔG(H2O) kJ/mol	73	178
m kJ/mol·M	23.8	45.6
chisq	0.11	0.071

FIGURE 3: Equilibrium unfolding of DCoH2 in GdnHCl as measured by intrinsic Trp fluorescence. (A) Guanidine unfolding of DCoH2 is at equilibrium after a 24 h incubation, as demonstrated by the coincidence of the unfolding (●) and refolding (Δ) curves at 2.1 μM DCoH2 concentration. Similar overlap was found at 0.5, 1.05, and 4.2 μM DCoH2 (not shown). Error bars show the standard deviation for three measurements. (B) Unfolding ΔG_{H_2O} and *m*-values for the best global fits to dimer-to-monomer and tetramer-to-monomer two-state models. The overall chi-squared values indicate similar goodness of fit for both models. (C) Normalized unfolding data of 0.5 μM (△), 1.05 μM (×), 2.1 μM (●), and 4.2 μM (□) DCoH2. The best global fit of the tetramer-to-monomer model ($N_4 \leftrightarrow 4U$) for 0.5 μM (− −), 1.05 μM (-·-·-), 2.1 μM (—), and 4.2 μM (---) DCoH2. Y_{tot} is the normalized fluorescence signal. (D) The best global fit of the dimer-to-monomer model ($D_2 \leftrightarrow 2U$). Symbols are the same as in (C). Error bars are shown for the 0.5 and 4.2 μM protein concentration data.

Table 2: Buried Surface Area versus *m*-Values

		buried surface (Å^2)[a]	calcd *m*-value[b] (kJ/(mol·M))	fit *m*-value (kJ/(mol·M))
DCoH2	monomer	9371		
	dimer interface	1549		
	dimer total	20291	23.5	23.8
	tetramer interface	2435		
	tetramer total	43017.6	45.4	45.6
DCoH1 T51S	monomer	10212		
	dimer interface	1364		
	dimer total	21787	25.0	38
	tetramer interface	2385		
	tetramer total	45961	48.2	85

[a]Buried surface area of oligomers calculated, e.g., for tetramer: 2(ASA dimer) − (ASA tetramer) (*52*). Buried surface area of monomers calculated as the sum of amino acid surfaces not accessible. [b]Calculated *m*-value according to the formula 953 + 0.23 (ΔASA) in kcal/(mol·M) (*51*).

The red shift of the tryptophan emission maxima and lower emission intensity is characteristic of increased solvent exposure upon denaturation (*53*).

DCoH2 Unfolding Is Reversible. Unfolding and refolding profiles for DCoH2 overlapped after 24 h (Figure 3A). GdnHCl-induced unfolding of DCoH2 was measured over an 8-fold protein concentration range: 0.5, 1.05, 2.1, and 4.2 μM DCoH2. The equilibrium unfolding is concentration dependent, as expected for oligomers (*49*, *54*). We expected the unfolding of the DCoH homotetramer to follow a three-state mechanism with a dimeric intermediate, yet the equilibrium unfolding curves contained a single cooperative transition. We therefore fit the data to two-state models (Figure 3B). The native folded state of DCoH is tetrameric, as demonstrated by the crystal structure and analytical ultracentrifugation (*7*, *32*, *55*). The data were modeled to a tetramer-to-monomer transition ($N_4 \leftrightarrow 4U$) (Figure 3C). The positive slope at low GdnHCl concentrations was fit as a linear baseline effect as a result of increasing salt (*56*). Given that the DCoH1 dimer interacts with HNF-1α, we also modeled the data as a dimer-to-monomer transition ($D_2 \leftrightarrow 2U$) (Figure 3D). The data fit these two models similarly, with an overall chi-squared value of 0.071 and 0.11 (Figure 3B). The *m*-values (24 kJ/(mol M) for the dimer-to-monmer model and 45.6 kJ/(mol M) for the tetramer-to-monomer model) were both close to the expected values calculated from the change in accessible surface area (Table 2) (*51*).

DCoH1 Unfolding Exhibits Hysteresis. GdnHCl unfolding and refolding of DCoH1, at 2.1 μM monomer concentration, exhibited hysteresis after a 24 h incubation time (Figure 4A). The midpoint of the unfolding curve is 3 M GdnHCl while refolding occurs at a much lower GdnHCl concentration, at about 1.25 M GdnHCl. An unfolding time course over 7 days revealed a slight decrease in the unfolding transition, to 2.8 M GdnHCl (not shown). A 3 day time course indicated no change in the refolding curve.

The DCoH1 Thr 51 Ser Point Mutant Unfolds Reversibly. We had previously proposed the difference in apparent stability between the DCoH1 and DCoH2 homotetramers might be due to Thr 51 in DCoH1 instead of Ser 51 in DCoH2 (*9*). While this is a conservative change, residue 51 is located at the center of the hydrophobic core of the tetramer interface. The less bulky Ser side chain allows for binding of an ordered water molecule within the hydrophobic core. Other differences between the tetrameric interfaces consist of solvent-exposed hydrophilic

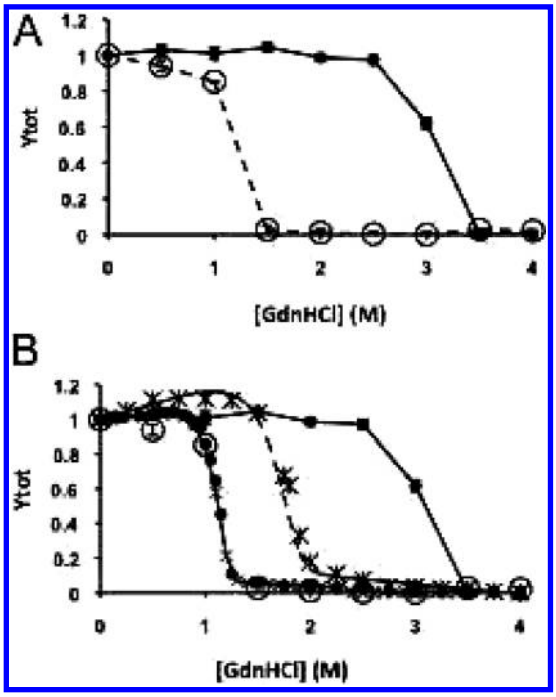

FIGURE 4: Unfolding of wild-type DCoH1 is not reversible. (A) Unfolding (■) and refolding (○) of DCoH1 were measured after 24 h at 2.1 μM protein concentration. Error bars are shown for three measurements and are about the size of the symbols. The unfolding transition (midpoint) occurs at about 3 M GdnHCl, significantly higher than the refolding transition (about 1.25 M GdnHCl). After 7 days the unfolding transition shifted by about 0.2 M GdnHCl lower (not shown). (B) Comparison of wild-type DCoH1 folding and refolding (as in (A)) with DCoH1 T51S data (●) with the tetramer-to-monomer fit (—) and DCoH2 data (×) with the tetramer-to-monomer fit (– –). The concentration of DCoH in each case is 2.1 μM. Refolding of wild-type DCoH1 coincides with the reversible folding of DCoH1 T51S. DCoH2 is more stable to guanidine unfolding than DCoH1 T51S, as measured by Trp fluorescence.

residues surrounding the hydrophobic core (*23*, *32*). We generated the DCoH1 Thr 51 Ser mutation to investigate whether Thr 51 contributes to the stability of DCoH1 to GdnHCl unfolding.

In order to confirm the presence of the interfacial water molecule in DCoH1 T51S, we determined the crystal structure at 1.8 Å resolution (Table 1). As expected, the electron density demonstrated the presence of the water molecule as found in DCoH2 (Figure 5). Ser 51 in DCoH1 T51S adopts the same two alternate conformations as in wild-type DCoH2. In one conformation the Ser hydroxyl forms bifurcated hydrogen bonds with the water molecule and the carbonyl oxygen of the $i - 4$ residue of the α helix, Phe 47. In the other conformation the Ser hydroxyl forms a bifurcated hydrogen bond with the Ser 51 side chain across the tetramer interface and the carbonyl oxygen of Gly 48 along the helix. Also in the center of the tetramer interface is a 37 Å^3 cavity, indicating the interface is not as tightly packed as it could be (Figure 6).

In stark contrast to the wild-type DCoH1, DCoH1 T51S unfolding is reversible. Unfolding and refolding curves overlapped after 24 h of equilibration (Figure 7A). Figure 7 shows the GdnHCl-induced unfolding data of DCoH1 T51S measured over an 8-fold protein concentration range between 0.5 and 4.2 μM. Like DCoH2, no intermediate could be detected in the unfolding curves. The data were fit to two two-state models: tetramer-to-unfolded monomer and dimer-to-unfolded monomer (Figure 7B−D). Unlike DCoH2 unfolding, the slope at low GdnHCl concentration for DCoH1 T51S unfolding was minimal, indicating that the positive slope

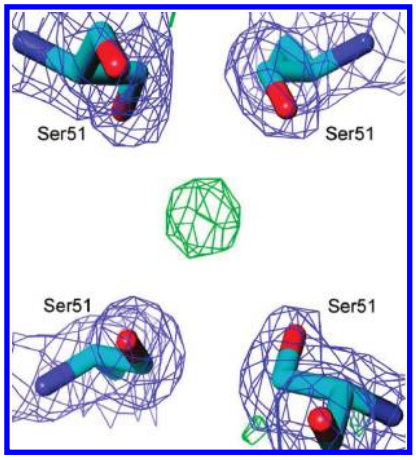

FIGURE 5: An ordered water molecule binds at the tetramer interface of DCoH1 T51S. The $F_o - F_c$ omit map (green, center), contoured at 3σ, indicates the position of the coordinated water. The $2F_o - F_c$ map (blue) is shown contoured at 1σ around the four Ser residues at position 51, one from each monomer. This water molecule is also present in DCoH2 but not wild-type DCoH1.

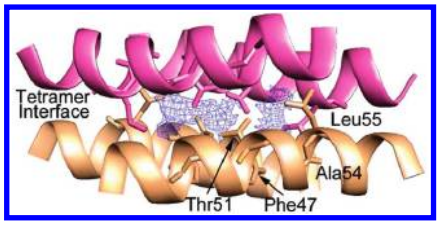

FIGURE 6: The tetramer interface of DCoH1 is not tightly packed. The primary interface between dimers (pink, beige) consists of a four-helix bundle, with one helix contributed from each monomer (ribbon representation). The cavity at the dimer−dimer interface was generated by the program Voidoo (*46*) with a 0.8 Å probe and has a total volume of ~37 Å^3 (mesh). This volume is too small to hold a water molecule but shows that the side chains are not tightly packed in the center of the interface. Residues bordering the cavity are shown as stick figures and are labeled for one monomer. A similar cavity is present in the DCoH2 and DCoH1 T51S tetramer interfaces. Coordinates for DCoH1 from PDB id 1DCP (*67*).

resulted from local effects on Trp 7 of DCoH2 (Figure 1). The best global fit was slightly better for the tetramer-to-monomer model (chi-squared value of 0.076) than for the dimer-to-monomer model (chi-squared value of 0.14) (Figure 7B). The *m*-values derived from the fit to the data (38 kJ/(mol·M) for the dimer-to-monomer model and 85 kJ/(mol·M) for the tetramer-to-monomer model) were greater than the expected values based on buried surface area (25 kJ/(mol·M) and 48 kJ/(mol·M), respectively, Table 2) (*51*).

Size Exclusion Chromatography. The oligomeric state of DCoH was evaluated by SEC as a function of GdnHCl concentration. Interpretation of the results was complicated by the salt dependence of the elution volume (*57*). To compare elution profiles at different GdnHCl concentrations, the DTT peaks were used as a reference (Figure 8). The TSK Super SW2000 column showed a greater dependence on ionic strength than the Biosep-SEC-S3000 column, as suggested by the elution volume of DTT. GdnHCl concentrations for SEC samples were chosen according to the transitions identified in the unfolding curves measured by intrinsic tryptophan fluorescence. For each transition two guanidine concentrations were measured: one corresponding to the edge of the "plateau", i.e., at a guanidine concentration just lower than the beginning of the transition, and at the midpoint of the transition.

Elution profiles for DCoH2 were measured with the TSK Super SW2000 column: at low GdnHCl (0.5 M GdnHCl), near the edge of the folded plateau (1.25 M GdnHCl), in the middle of the unfolding transition (1.8 M GdnHCl), and unfolded (4 M GdnHCl) (Figure 9A). The elution profiles were similar for the Biosep-SEC-S3000 column (not shown). The peak at 0.5 M GdnHCl eluted slower than the expected molecular mass of a tetramer (near 35 kDa instead of 48 kDa) (Figure 9A, level 1). The 1.25 M GdnHCl peak eluted before the tetramer peak, and the 1.8 M GdnHCl peak eluted after the tetramer peak (Figure 9A, level 2). The unfolded DCoH2 monomer peak at 4 M GdnHCl eluted similar to the tetramer peak (Figure 9A, level 3). This is likely due to a combination of the increased salt concentration and the extended size of the unfolded monomer. The overall difference in the elution volume between peaks was less than expected for the tetrameric, dimeric, and monomeric species based on the molecular mass standards. While it is difficult to interpret the identity of these species, the elution peaks suggest the existence of two unfolding intermediates.

Elution profiles of wild-type DCoH1 were measured with the TSK Super SW2000 column after 24 h of equilibration (Figure 9B). Since DCoH1 unfolding showed hysteresis, unfolding and refolding samples were compared. The 0 M GdnHCl and 0.15 M GdnHCl samples represent the folded tetramer. The 0 M GdnHCl sample eluted anomalously due to the low salt buffer (50 mM potassium phosphate, pH 7.4) (Figure 9B, level 1). This was confirmed on the Biosep-SEC-S3000 column by rerunning the 0 M GdnHCl sample with 0.15 M NaCl, which eluted like the 0.15 M GdnHCl sample (Figure 9C, level 1). Unfolding and refolding samples were prepared at 0.7 M GdnHCl and 1.25 M GdnHCl, corresponding to the refolding transition identified by tryptophan fluorescence (Figure 4A). The elution peaks for these GdnHCl concentrations were slightly after (0.7 M GdnHCl) and slightly before (1.25 M GdnHCl) the 0.15 M GdnHCl tetramer peak, suggestive of a transition (Figure 9B, level 2). Surprisingly, the hysteresis measured by fluorescence was not apparent in the elution profiles, since the refolding and unfolding profiles were identical. The second transition was at 2.75 and 3 M GdnHCl, corresponding to unfolding of wild-type DCoH1 as measured by tryptophan fluorescence. The profiles were identical for both guanidine concentrations, eluting as two peaks (Figure 9B, level 3). The larger peak eluted like the unfolded monomer at 4 M GdnHCl (Figure 9B, level 4).

The same samples were rerun on the Biosep-SEC-S3000 column 10 days later. The silica matrix of the Biosep column is coated to minimize charge interactions. This is meant to allow proteins to elute according to their molecular mass in the presence of high salt (*57*). Despite this, the elution profiles were similar to those of the TSK Super SW2000. The peaks still did not correspond to the elution volumes of a tetramer, dimer, or monomer as defined by the standard curve (Figure 9C). Two changes in the elution profiles were apparent after 10 days of equilibration. The first transition (between 0.7 and 1.25 M GdnHCl) now appeared as a single species (compare Figure 9B and Figure 9C, level 2). The second transition appeared as a single peak instead of a double peak, transitioning completely to the unfolded monomer for both the 2.75 and 3 M GdnHCl unfolding samples (compare Figure 9B and Figure 9C, level 3).

In order to further test whether we could observe hysteresis by SEC, we measured the elution profile of DCoH1 refolded to 2.75 M GdnHCl. By tryptophan fluorescence the sample appeared to be completely unfolded, while the unfolding sample appeared

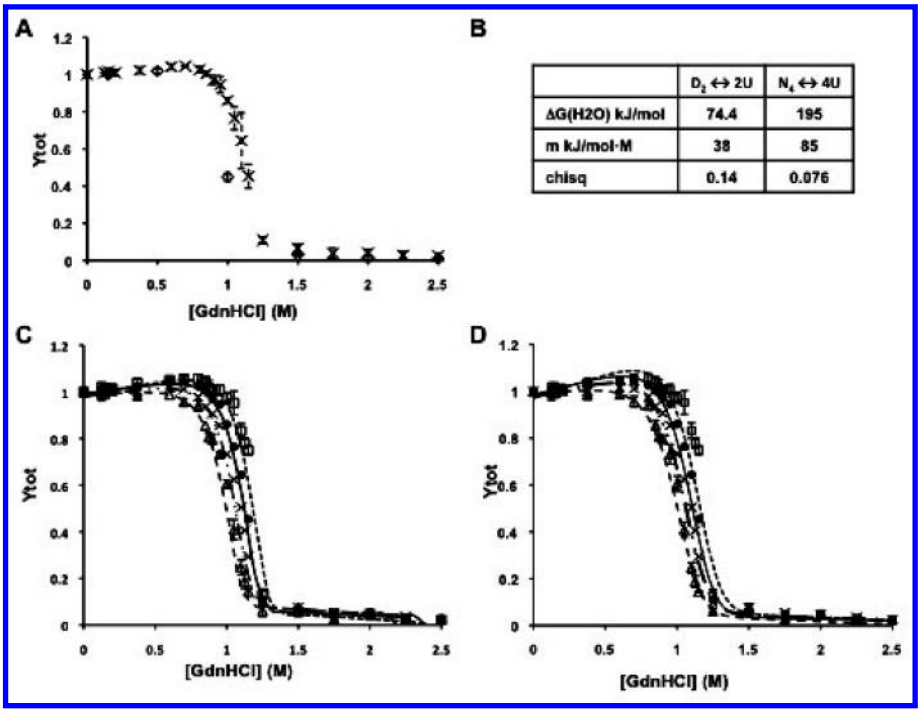

FIGURE 7: Equilibrium unfolding of DCoH1 T51S in GdnHCl as measured by intrinsic Trp fluorescence. (A) Guanidine unfolding of DCoH1 T51S is at equilibrium after a 24 h incubation, as demonstrated by the coincidence of the unfolding (×) and refolding (○) curves at 2.1 μM DCoH1 T51S concentration. Similar overlap was found at 0.5, 1.05, and 4.2 μM DCoH1 T51S (not shown). Error bars show the standard deviation of three measurements. (B) Unfolding ΔG_{H_2O} and *m*-values for the best global fits to dimer-to-monomer and tetramer-to-monomer two-state models. The overall chi-squared values indicate similar goodness of fit for both models. (C) Normalized unfolding data at 0.5 μM (△), 1.05 μM (×), 2.1 μM (●), and 4.2 μM (□) DCoH1 T51S. The best global fit to the tetramer-to-monomer model ($N_4 \leftrightarrow 4U$) for 0.5 μM (− −), 1.05 μM (-···-), 2.1 μM (—), and 4.2 μM (---) DCoH1 T51S. Y_{tot} is the normalized fluorescence signal. Error bars are shown for the 0.5 and 4.2 μM protein concentration data. (D) The best global fit of the dimer-to-monomer model ($D_2 \leftrightarrow 2U$). Symbols are the same as in (C).

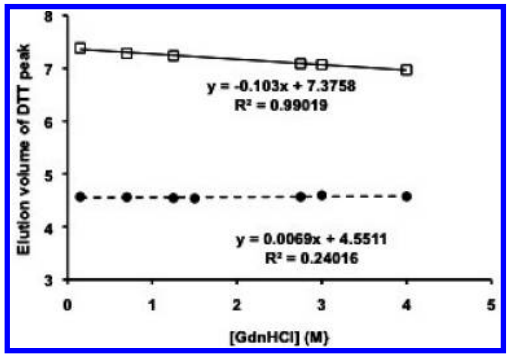

FIGURE 8: Elution volumes for the DTT peak on the TSK-GEL Super SW2000 column (□) and the Biosep-SEC-S3000 column (●) at different guanidine concentrations. The TSK-GEL SW2000 column showed a stronger dependence on ionic strength than did the Biosep-SEC-S3000 column. Also shown is the fit to a line, as calculated by Excel (Microsoft).

to be completely folded (Figure 4A). After refolding for 1 day, this sample eluted identically to the unfolding samples at 2.75 M GdnHCl (compare Figure 9B and Figure 9C, level 3). In other words, no hysteresis was apparent by SEC.

The elution profiles for the unfolding transition of DCoH1 T51S at 0.7 and 1.15 M GdnHCl were identical to the wild-type DCoH1 profiles at 0.7 and 1.25 M GdnHCl (compare Figure 9D, levels 1 and 2). This suggests that the same intermediates are accessible to wild-type DCoH1 and DCoH1 T51S.

DCoH1 T51S Binds to HNF-1α in Vitro. In order to test whether the T51S mutation enhances interaction of DCoH1 with HNF-1α, we conducted a pull-down assay with HNF-1α 1−280-His_6 (Figure 10). Similar to DCoH2, DCoH1 T51S now interacts with HNF-1α *in vitro* through simple mixing. Since the T51S mutation is situated in the tetramer interface, this implies that formation of the HNF-1α complex with wild-type DCoH1 is hindered by the stability of the homotetramer.

DISCUSSION

We present the first quantitative measurements of DCoH homotetramer stability. These measurements are important for understanding the regulation of DCoH's two apparently unrelated functions, as a metabolic enzyme in the cytoplasm and as a transcriptional coactivator in the nucleus (*6*, *8*). These studies elaborate the differences in the stability of the two vertebrate paralogues, DCoH1 and DCoH2 (*17*, *32*). While DCoH1 is resistant to unfolding by heat and up to 8 M urea (not shown), DCoH1 and DCoH2 unfold readily in 4 M GdnHCl. GdnHCl can interact with side chains, modifying the pK_a and neutralizing charge interactions (*23*, *56*, *58*, *59*). In agreement with the role of charge interactions, low pH enhanced unfolding of DCoH1 (data not shown). DCoH1 and DCoH2 unfold in a single transition, as measured by intrinsic tryptophan fluorescence (Figures 3 and 4). DCoH1 is more resistant to GdnHCl unfolding than DCoH2 (3 versus 1.8 M) (Figure 4B). DCoH1 unfolding does not reach equilibrium after 7 days but shows a pronounced hysteresis in which the refolding occurs at a much lower GdnHCl concentration (1.25 M GdnHCl).

The single point mutation in DCoH1 of Thr 51 to Ser, as in DCoH2, overcomes the unfolding hysteresis of wild-type DCoH1 (Figure 7). The structure of DCoH1 T51S is a homotetramer, like DCoH1 and DCoH2. Thr 51 is located at the center of the hydrophobic tetramer interface, placing the four Thr 51 residues

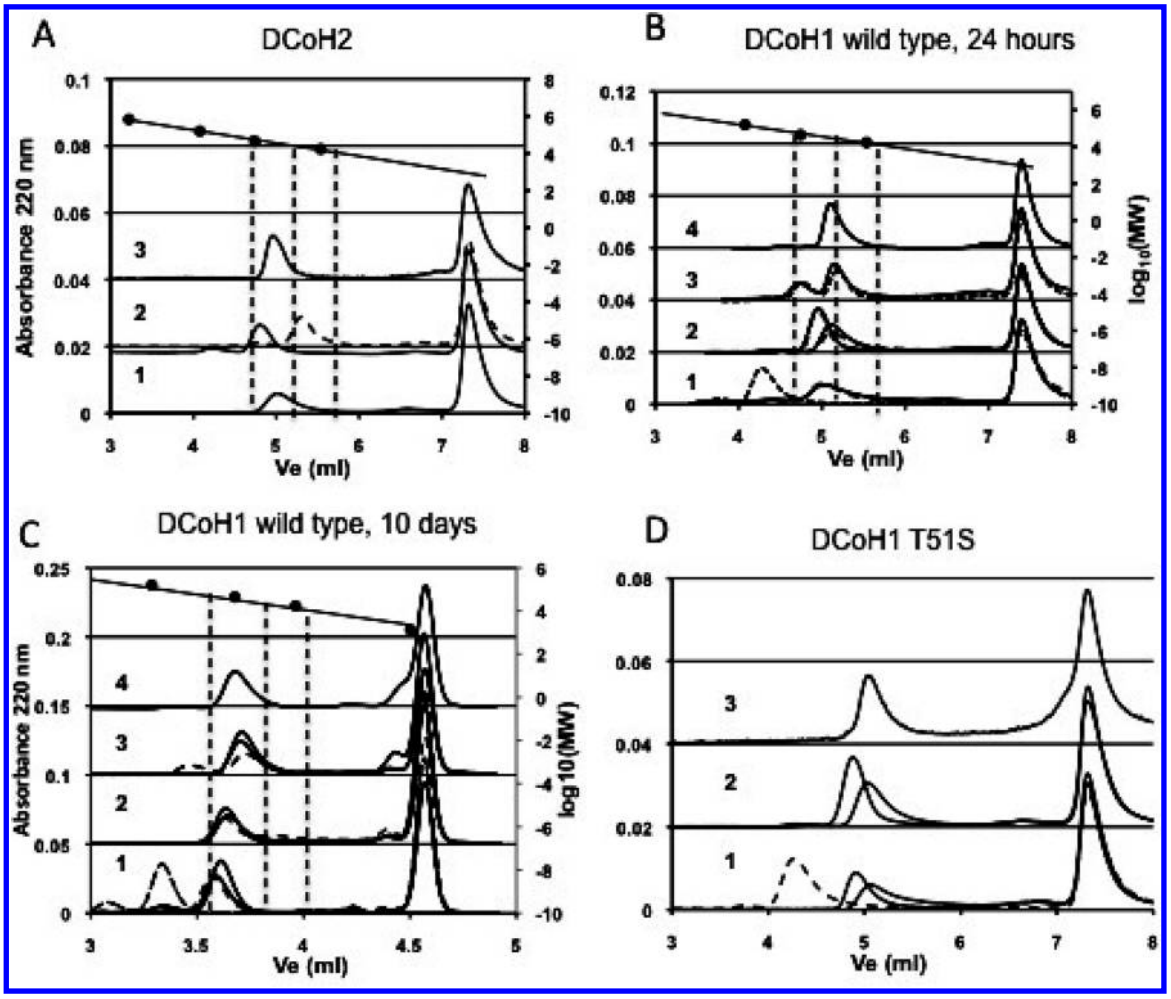

FIGURE 9: Size exclusion chromatography elution profiles of GdnHCl unfolded (A) DCoH2, (B, C) wild-type DCoH1, and (D) DCoH1 T51S. Profiles have been translated vertically for comparison and labeled as levels 1−4 on the figure. (A) DCoH2. Level 1, 0.5 M GdnHCl; level 2, 1.25 M (—) and 1.8 M (− −) GdnHCl; level 3, 4 M GdnHCl. (B) Wild-type DCoH1 after 24 h equilibration. Unless otherwise specified, the unfolding samples are depicted as (—) and the refolding samples are depicted as (− −). Level 1, 0 M GdnHCl (left peak, − −), 0.15 M GdnHCl unfolding and refolding (right peaks). Level 2, 0.7 M (right peak) and 1.25 M GdnHCl (left peak). Level 3, 2.75 and 3 M GdnHCl unfolding. Both profiles are doublets. Level 4, 4 M GdnHCl peak. (C) Wild-type DCoH1 after 10 days of equilibrium. Unless otherwise specified, the unfolding samples are depicted as (—) and the refolding samples are depicted as (− −). Level 1, 0 M GdnHCl (left peak, − −), 0 M GdnHCl plus 0.15 M NaCl (right-most peak, —), 0.15 M GdnHCl unfolding and refolding. The 0 M GdnHCl peak runs anomalously due to the low salt. Level 2, 0.7 and 1.25 M (folding and unfolding) GdnHCl. The profiles are now coincident. Level 3, 2.75 and 3 M GdnHCl unfolding and 2.75 M GdnHCl refolding after 24 h of equilibration. Level 4, 4 M GdnHCl. (D) DCoH T51S. Level 1, 0 M GdnHCl (left, − −), 0.7 M (right) and 1.15 M GdnHCl (middle peak). Level 2, wild-type DCoH1 peaks at 0.7 and 1.25 M GdnHCl after 24 h of equilibration. These peaks elute at the same volume as the 0.7 and 1.15 M GdnHCl DCoH1 T51S peaks (level 1). Level 3, 4 M GdnHCl. Profiles have been translated so the DTT peaks (right peak of each profile) overlap with the DTT peak of the lowest guanidine concentration sample greater than 0 M GdnHCl. The left vertical axis shows the absorbance of the elution profiles at 220 nm. The right vertical axis shows the log of the molecular weight (MW) from the standards. The vertical dotted lines indicate the elution volumes (from left to right) of a DCoH tetramer (48 kDa), dimer (24 kDa), and monomer (12 kDa), as predicted from the linear fit to log (MW) of the standards (●). Elution volumes are measured in mL. (A), (B), and (D) used the TSK-GEL Super SW2000 column. (C) used the Biosep-SEC-S3000 column.

from each DCoH1 monomer in close proximity. Like DCoH2, a buried water molecule is positioned in the center of the DCoH1 T51S structure, hydrogen bonding with the Ser 51 side chains (Figure 5). It is difficult to predict the energetic cost of the T51S mutation. As has been noted elsewhere, the energetic cost of ordering a water molecule can be compensated by the formation of hydrogen bonds, in this case to the water molecule and across the tetramer interface (*60*). Even so, the T51S mutation significantly reduces the guanidine concentration required for unfolding DCoH1.

Because Thr 51 is positioned in the tetramer interface, the Ser mutation most likely destabilizes the DCoH1 homotetramer. DCoH1 T51S unfolds reversibly with a folding midpoint around 1.15 M GdnHCl, similar to the refolding of wild-type DCoH1 (Figure 4B). This suggests that the refolding transition for wild-type DCoH1 occurs at the same step in the folding pathway as the reversible folding of DCoH T51S. This could be the case if the single transition represents dimer-to-monomer folding, as depicted in Scheme 1. In this scheme, unfolded monomers fold reversibly to a dimer burying the Trp residues. Unfolding of the wild-type DCoH1 tetramer is slow, explaining the hysteresis.

$$N_4 \xrightarrow{\text{slow}} 2D_2 \leftrightarrow U \qquad \text{(Scheme 1)}$$

We consider the dimer to be the most likely unfolding intermediate because (1) the dimer buries significant surface area (1360−1550 Å^2 plus hydrogen bonds across the β-sheet at the dimer interface; Table 2 and Figure 1); (2) the prokaryotic

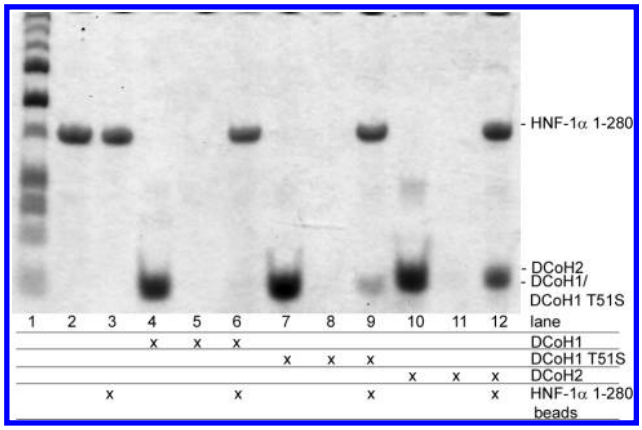

FIGURE 10: DCoH1 T51S interacts with HNF-1α *in vitro*. HNF-1α 1−280-His_6 was immobilized on nickel affinity resin (lane 3) and incubated with purified DCoH1, DCoH1 T51S, or DCoH2. DCoH1 T51S and DCoH2 bind to HNF-1α 1−280 (lanes 9 and 12) unlike DCoH1 wild type (lane 6). DCoH proteins did not bind to the beads alone (lanes 5, 8, and 11). DCoH and HNF-1α loads are shown in lanes 2, 4, 7, and 10. Protein standards (Bio-Rad Precision Plus) are shown in lane 1.

DCoH, PhhB, is dimeric (*61*); (3) a DCoH dimer interacts with HNF-1α (*3*, *9*); and (4) a dimer of DCoH2 has been reported by size exclusion chromatography (*15*). The DCoH2 and DCoH1 T51S equilibrium unfolding curves fit a dimer- or tetramer-unfolding model almost as well (Figures 3 and 7). For DCoH2 both the dimer-unfolding and tetramer-unfolding models predict reasonable *m*-values (Figure 3B, Table 2). For DCoH1 T51S, the *m*-value for the tetramer-unfolding model was much larger than expected (Figure 7B, Table 2). The *m*-value for the dimer-unfolding model was more reasonable (Table 2). The intermediate cannot be a monomer since folding of DCoH1 T51S is concentration dependent.

DCoH2 is more stable to guanidine unfolding than DCoH1 T51S (Figure 4B). This was unexpected given the greater apparent stability of wild-type DCoH1. The tetramer interfaces of DCoH1 T51S and DCoH2 are mostly conserved, particularly the hydrophobic cores (*32*). Two hydrogen bonds across the tetramer interface (Lys 59 to Asp 61 and Arg 45 to Gln 98) have been proposed to stabilize the DCoH1 homotetramer (*23*). These interactions are accessible in the DCoH1 T51S mutant as in wild-type DCoH1, yet none of these hydrogen bonds form in the DCoH T51S structure. Comparing the structures of DCoH1 and DCoH2 indicates a large number of charge−charge interactions and hydrogen bonds on the monomer surfaces that could be disrupted by GdnHCl (Supporting Information Table S1). The greater stability of DCoH2 to guanidine denaturation, as measured by Trp fluorescence, may therefore reflect greater stability of the dimer and not the tetramer.

Folding Intermediates Detected by Size Exclusion Chromatography. Size exclusion chromatography was carried out to identify intermediates not observable by intrinsic Trp fluorescence. The elution profiles varied at different guanidine concentrations (Figure 9). The peaks all eluted between the predicted molecular masses of a tetramer and a dimer, including the unfolded monomer. The peaks might elute anomalously because of the shape of the protein or changes in ionic strength due to guanidine. According to Tosoh, the optimal mobile phase for the TSK-GEL SW columns is between 0.1 and 0.5 M ionic strength to avoid ionic or hydrophobic interactions with the silica matrix. The Biosep-SEC S3000 silica support is coated with a hydrophilic coating to minimize interactions (*62*). The effect of ionic strength on interactions with the matrix was apparent in the variation of the retention times of the DTT peak at different GdnHCl concentrations (Figure 8). The variation was less for the Biosep-SEC S3000 column, but was detectable. To compare chromatograms at different GdnHCl concentrations, we aligned the DTT peaks. This is a crude approximation since DCoH does not share the same hydrophobic and ionic characteristics as DTT. Nevertheless, the elution profiles were similar with both columns, suggesting the position of the peaks were independent of interactions with the matrix.

The elution profiles may also depend on the flow rate through the column (*63*). For a complex, the elution peaks reflect the initial equilibrium conditions of the sample if the on-rate and off-rate of the complex are slow relative to the column elution time (*63*). In contrast, if equilibration of the complex is instantaneously fast, a single peak will elute midway between the complex and the free constituents. For instantaneously fast conditions the peak shape is characteristically skewed with a sharp leading edge and an elongated trailing edge, like the shape of the 0.7 M GdnHCl peak (Figure 9B, level 2). At off-rates slower than instantaneous but still fast, the peak position may shift toward the free constituents or may elute as two peaks, depending on the on-rate and the flow rate of the mobile phase. The linear flow rate through these columns is 2 cm/min, at a flow rate of 0.35 mL/min. Stevens proposed that a half-life of a complex less than 5−10% of the run time of the SEC column could result in two peaks, or for our columns an off-rate $>0.01\ s^{-1}$ for 20 min run times (*63*). These effects may be particularly relevant to chemical denaturation studies since the off-rate of the complex can increase as the dissociation constant increases at higher guanidine concentrations.

Our elution series minimally represent two folding intermediates for DCoH1 and DCoH2: one eluting after the tetramer peak and one eluting before the tetramer peak. The identity of these species is not yet known, but a few observations are notable. First, there is no apparent hysteresis in the unfolding of wild-type DCoH1 by SEC, at 0.7 M GdnHCl or at 2.75 M GdnHCl. In order to reconcile this with the pronounced hysteresis detected by Trp fluorescence, we propose that the peak at 0.7 M GdnHCl must represent an intermediate (I_4) that is accessible via unfolding and refolding, for example, Scheme 2:

$$N_4 \overset{\text{fast}}{\leftrightarrow} I_4 \underset{\text{fast}}{\overset{\text{slow}}{\rightleftharpoons}} 2D_2 \leftrightarrow I_1 \leftrightarrow U \qquad \text{(Scheme 2)}$$

where I_4 was detected by Trp fluorescence.

Hysteresis could result from slow unfolding of I_4. The peak at 2.75 M GdnHCl must be an intermediate (I_1) with no tryptophan fluorescence, given that it is not detected by fluorescence during refolding. In this scheme, the transition from I_1 to the dimer (D_2) represents the reversible folding step identified by Trp fluorescence in Scheme 1. Further studies are required to characterize these intermediates.

There are two time-dependent transitions in the unfolding of wild-type DCoH1. After equilibrating for 1 day, the peaks at 0.7 and 1.25 M GdnHCl eluted separately (Figure 9B, level 2), and the peak at 2.75 and 3 M GdnHCl eluted as a doublet (Figure 9B, level 3). After 10 days the peaks at 0.7 and 1.25 M GdnHCl eluted together (Figure 9C, level 2), and the doublet at 2.75 and 3 M GdnHCl eluted as a single peak (Figure 9C, level 3). These time-dependent changes support the possibility of kinetically slow

steps in DCoH1 unfolding. The DCoH1 homotetramer may be kinetically stable, rather than thermodynamically stable (*33*, *64*). Other examples of kinetic stability of oligomers have been identified, such as thermophilic alcohol dehydrogenase and transthyretin (*65*, *66*).

Implications for DCoH Regulation of HNF-1. Formation of the DCoH1/HNF-1α complex requires cofolding (*3*, *9*, *31*). The hysteresis in DCoH1 unfolding suggests that the wild-type DCoH1 homotetramer is essentially trapped once it forms. Refolding of the DCoH1 dimer appears to be reversible, as with DCoH1 T51S, allowing interaction with HNF-1α. In liver cells, the DCoH1 concentration (low micromolar) far exceeds the concentration of HNF-1α (nanomolar) (*3*, *15*, *17*, *24*, *25*). Due to the stability of the DCoH1 homotetramer, the general pool of DCoH1 may not be available to interact with HNF-1α. As a result, complex formation may depend on newly translated DCoH1 in proximity to HNF-1α dimers in the cytoplasm. Because the DCoH2 dimer is more stable than the DCoH1 dimer, formation of DCoH2/HNF-1α complexes may be favored over DCoH1/HNF-1α complexes if DCoH2 is present.

Future Studies. As a first step in understanding the process of DCoH1/HNF-1 cofolding, we are characterizing the folding pathway of the DCoH1 and DCoH2 homotetramers. Further studies are required to understand the unfolding hysteresis of DCoH1 and whether it has a thermodynamic or kinetic origin (*33*, *64*). We predict that the unfolding of the wild-type DCoH1 homotetramer will not be concentration dependent, if it depends on the off-rate of the tetramer alone. One unanswered question is the concentration dependence of the intermediates identified by SEC. Finally, kinetic studies will be needed to characterize the folding pathway and, ultimately, formation of the DCoH1/HNF-1α complex.

ACKNOWLEDGMENT

We thank Clay Clark for insightful discussions. We thank Michelle Dechene for X-ray data collection, Paul Swartz for assistance with solving the structure, and Sara Milam for helpful discussions about initial folding experiments. Data were collected at Southeast Regional Collaborative Access Team (SER-CAT) 22-BM beamline at the Advanced Photon Source, Argonne National Laboratory. Supporting institutions may be found at www.ser-cat.org/members.html.

SUPPORTING INFORMATION AVAILABLE

The equations used to fit the tetramer-to-monomer model (Figure S1), Igor Pro algorithms used for fitting the data to the tetramer-to-monomer and dimer-to-monomer unfolding models (Figure S2), the best parameters for the global fit to the tetramer-to-monomer and dimer-to-monomer models, including baseline fits (Figure S3), and a table listing hydrogen-bonding and charge interactions that stabilize the DCoH1 and DCoH2 dimers (Table S1). This material is available free of charge via the Internet at http://pubs.acs.org.

REFERENCES

1. Chan, H. M., and La Thangue, N. B. (2001) p300/CBP proteins: HATs for transcriptional bridges and scaffolds. *J. Cell Sci. 114*, 2363–2373.
2. Vo, N., and Goodman, R. H. (2001) CREB-binding protein and p300 in transcriptional regulation. *J. Biol. Chem. 276*, 13505–13508.
3. Mendel, D., Khavari, P., Conley, P., Graves, M., Hansen, L., Admon, A., and Crabtree, G. (1991) Characterization of a cofactor that regulates dimerization of a mammalian homeodomain protein. *Science 254*, 1762–1767.
4. Spiegelman, B. M., and Heinrich, R. (2004) Biological control through regulated transcriptional coactivators. *Cell 119*, 157–167.
5. Beckett, D. (2004) Functional switches in transcription regulation: molecular mimicry and plasticity in protein-protein interactions. *Biochemistry 43*, 7983–7991.
6. Citron, B., Davis, M., Milstien, S., Gutierrez, J., Mendel, D., Crabtree, G., and Kaufman, S. (1992) Identity of 4a-carbinolamine dehydratase, a component of the phenylalanine hydroxylation system, and DCoH, a transregulator of homeodomain proteins. *Proc. Natl. Acad. Sci. U.S.A. 89*, 11891–11894.
7. Endrizzi, J., Cronk, J., Wang, W., Crabtree, G., and Alber, T. (1995) Crystal structure of DCoH, a bifunctional, protein-binding transcriptional coactivator. *Science 268*, 556–559.
8. Hauer, C., Rebrin, I., Thony, B., Neuheiser, F., Curtius, H., Hunziker, P., Blau, N., Ghisla, S., and Heizmann, C. (1993) Phenylalanine hydroxylase-stimulating protein/pterin-4α-carbinolamine dehydratase from rat and human liver. Purification, characterization, and complete amino acid sequence. *J. Biol. Chem.* 4828–4831.
9. Rose, R., Bayle, J., Endrizzi, J., Cronk, J., Crabtree, G., and Alber, T. (2000) Structural basis of dimerization, coactivator recognition and MODY3 mutations in HNF-1alpha. *Nat. Struct. Biol. 7*, 744–748.
10. Huang, C. Y., and Kaufman, S. (1973) Studies on the mechanisms of action of phenylalanine hydroxylase and its protein stimulator. I. Enzyme concentration dependence of the specific activity of phenylalanine hydroxylase due to a nonenzymatic step. *J. Biol. Chem. 248*, 4242–4251.
11. Rebrin, I., Bailey, S. W., and Ayling, J. E. (1995) Activity of the bifunctional protein 4a-hydroxy-tetrahydropterin dehydratase/DCoH during human fetal development: correlation with dihydropteridine reductase activity and tetrahydrobiopterin levels. *Biochem. Biophys. Res. Commun. 217*, 958–965.
12. Kaufman, S. (1970) A protein that stimulates rat liver phenylalanine hydroxylase. *J. Biol. Chem. 245*, 4751–4759.
13. Kaufman, S. (1993) New tetrahydrobiopterin-dependent systems. *Annu. Rev. Nutr. 13*, 261–286.
14. Citron, B. A., Kaufman, S., Milstien, S., Naylor, E. W., Greene, C. L., and Davis, M. D. (1993) Mutation in the 4a-carbinolamine dehydratase gene leads to mild hyperphenylalaninemia with defective cofactor metabolism. *Am. J. Hum. Genet. 53*, 768–774.
15. Hevel, J. M., Stewart, J. A., Gross, K. L., and Ayling, J. E. (2006) Can the DCoHalpha isozyme compensate in patients with 4a-hydroxy-tetrahydrobiopterin dehydratase/DCoH deficiency? *Mol. Genet. Metab. 88*, 38–46.
16. Thony, B., Neuheiser, F., Kierat, L., Rolland, M. O., Guibaud, P., Schluter, T., Germann, R., Heidenreich, R. A., Duran, M., de Klerk, J. B., Ayling, J. E., and Blau, N. (1998) Mutations in the pterin-4alpha-carbinolamine dehydratase (PCBD) gene cause a benign form of hyperphenylalaninemia. *Hum. Genet. 103*, 162–167.
17. Bayle, J., Randazzo, F., Johnen, G., Kaufman, S., Nagy, A., Rossant, J., and Crabtree, G. (2002) Hyperphenylalaninemia and impaired glucose tolerance in mice lacking the bifunctional DCoH gene. *J. Biol. Chem. 277*, 28884–28891.
18. Strandmann, E. P., Senkel, S., and Ryffel, G. U. (1998) The bifunctional protein DCoH/PCD, a transcription factor with a cytoplasmic enzymatic activity, is a maternal factor in the rat egg and expressed tissue specifically during embryogenesis. *Int. J. Dev. Biol. 42*, 53–59.
19. Pogge v Strandmann, E., and Ryffel, G. (1995) Developmental expression of the maternal protein XDCoH, the dimerization cofactor of the homeoprotein LFB1 (HNF1). *Development 121*, 1217–1226.
20. Pogge v Strandmann, E., Senkel, S., and Ryffel, G. (2000) Ectopic pigmentation in *Xenopus* in response to DCoH/PCD, the cofactor of HNF1 transcription factor/pterin-4alpha-carbinolamine dehydratase. *Mech. Dev. 91*, 53–60.
21. Yamagata, K., Oda, N., Kaisaki, P., Menzel, S., Furuta, H., Vaxillaire, M., Southam, L., Cox, R., Lathrop, G., Boriraj, V., Chen, X., Cox, N., Oda, Y., Yano, H., Le Beau, M., Yamada, S., Nishigori, H., Takeda, J., Fajans, S., Hattersley, A., Iwasaki, N., Hansen, T., Pedersen, O., Polonsky, K., Turner, R., Velho, G., Chevre, J., Froguel, P., and Bell, G. (1996) Mutations in the hepatocyte nuclear factor-1α gene in maturity-onset diabetes of the young (MODY3). *Nature 384*, 455–458.
22. Horikawa, Y., Iwasaki, N., Hara, M., Furuta, H., Hinokio, Y., Cockburn, B. N., Lindner, T., Yamagata, K., Ogata, M., Tomonaga, O., Kuroki, H., Kasahara, T., Iwamoto, Y., and Bell, G. I. (1997) Mutation in hepatocyte nuclear factor-1 beta gene (TCF2) associated with MODY. *Nat. Genet. 17*, 384–385.
23. Hevel, J. M., Pande, P., Viera-Oveson, S., Sudweeks, T. J., Jaffree, L. S., Hansen, C. M., and Ayling, J. E. (2008) Determinants of oligomerization of the bifunctional protein DCoHalpha and the effect

on its enzymatic and transcriptional coactivator activities. *Arch. Biochem. Biophys. 477*, 356–362.
24. Rebrin, I., Bailey, S. W., Boerth, S. R., Ardell, M. D., and Ayling, J. E. (1995) Catalytic characterization of 4a-hydroxytetrahydropterin dehydratase. *Biochemistry 34*, 5801–5810.
25. Chouard, T., Blumenfeld, M., Bach, I., Vandekerckhove, J., Cereghini, S., and Yaniv, M. (1990) A distal dimerization domain is essential for DNA-binding by the atypical HNF1 homeodomain. *Nucleic Acids Res. 18*, 5853–5863.
26. Lichtsteiner, S., and Schibler, U. (1989) A glycosylated liver-specific transcription factor stimulates transcription of the albumin gene. *Cell 57*, 1179–1187.
27. Lim, S., Jin, K., and Friedman, E. (2002) Mirk protein kinase is activated by MKK3 and functions as a transcriptional activator of HNF1alpha. *J. Biol. Chem. 277*, 25040–25046.
28. Kim, H., You, S., Foster, L., Farris, J., Choi, Y., and Foster, D. (2001) Differential expression of chicken dimerization cofactor of hepatocyte nuclear factor-1 (DCoH) and its novel counterpart, DCoHalpha. *Biochem. J. 354*, 645–653.
29. Cronk, J. (1996) Structural studies of DCoH, a bifunctional enzyme and protein-binding transcriptional coactivator, in Molecular and Cell Biology, University of California, Berkeley, Berkeley, CA.
30. Ficner, R., Sauer, U., Stier, G., and Suck, D. (1995) Three-dimensional structure of the bifunctional protein PCD/DCoH, a cytoplasmic enzyme interacting with transcription factor HNF1. *EMBO J. 14*, 2034–2042.
31. Johnen, G., and Kaufman, S. (1997) Studies on the enzymatic and transcriptional activity of the dimerization cofactor for hepatocyte nuclear factor 1. *Proc. Natl. Acad. Sci. U.S.A. 94*, 13469–13474.
32. Rose, R. B., Pullen, K. E., Bayle, J. H., Crabtree, G. R., and Alber, T. (2004) Biochemical and structural basis for partially redundant enzymatic and transcriptional functions of DCoH and DCoH2. *Biochemistry 43*, 7345–7355.
33. Sohl, J. L., Jaswal, S. S., and Agard, D. A. (1998) Unfolded conformations of alpha-lytic protease are more stable than its native state. *Nature 395*, 817–819.
34. Makarova, O., Kamberov, E., and Margolis, B. (2000) Generation of deletion and point mutations with one primer in a single cloning step. *BioTechniques 29*, 970–972.
35. Gasteiger, E., Hoogland, C., Gattiker, A., Duvaud, S., Wilkins, M. R., Appel, R. D., and Bairoch, A. (2005) Protein Identification and Analysis Tools on th ExPASy Server, in The Proteomics Protocols Handbook (Walker, J. M., Ed.) Humana Press, Totowa, NJ.
36. Gill, S. C., and von Hippel, P. H. (1989) Calculation of protein extinction coefficients from amino acid sequence data. *Anal. Biochem. 182*, 319–326.
37. Leslie, A. (1992) Recent changes to the MOSFLM package for processing film and image plate data, *Joint CCP4 and ESF-EAMCB Newsletter on Protein Crystallography* 26.
38. Collaborative Computation Project, N. (1994) The CCP4 suite: programs for protein crystallography. *Acta Crystallogr. D50*, 760–763.
39. Evans, P. (1993) Data reduction, in *Proceedings of CCP4 Study Weekend on Data Collection & Processing*, pp 114−122.
40. French, G., and Wilson, K. (1978) On the treatment of negative intensity observations. *Acta Crystallogr. A34*, 517.
41. Holton, J., and Alber, T. (2003) Automated protein crystal structure determination using ELVES. *Proc. Natl. Acad. Sci. U.S.A. 101*, 1537–1542.
42. Brunger, A., Adams, P., Clore, G., Delano, W., Gros, P., Grosse-Kunstleve, R., Jiang, J.-S., Kuszewski, J., Nilges, N., Pannu, N., Read, R., Rice, L., Simonson, T., and Warren, G. (1998) Crystallography and NMR system (CNS): a new software system for macromolecular structure determination. *Acta Crystallogr. D54*, 905–921.
43. Jones, T., Zhou, J., Cowan, S., and Kjeldgaard, M. (1991) Improved methods for building protein models in electron density maps and the location of errors in these models. *Acta Crystallogr. A47*, 110–119.
44. Emsley, P., and Cowtan, K. (2004) Coot: model-building tools for molecular graphics. *Acta Crystallogr., Sect. D: Biol. Crystallogr. 60*, 2126–2132.
45. Delano, W. (2002) The Pymol Molecular Graphics System.
46. Kleywegt, G. J., and Jones, T. A. (1994) Detection, delineation, measurement and display of cavities in macromolecular structures. *Acta Crystallogr., Sect. D: Biol. Crystallogr. 50*, 178–185.
47. Kleywegt, G. J., and Jones, T. A. Mapman, 080625 ed., Uppsala Software Factory, Uppsala.
48. Pace, C. N., and Scholtz, J. M. (1997) Measuring the conformational stability of a protein, in Protein Structure: A Practical Approach (Creighton, T. E., Ed.) 2nd ed., Oxford University Press, Oxford.
49. Walters, J., Milam, S. L., and Clark, A. C. (2009) Practical approaches to protein folding and assembly: spectroscopic strategies in thermodynamics and kinetics. *Methods Enzymol. 455*, 1–39.
50. Catanzano, F., Graziano, G., De Paola, B., Barone, G., D'Auria, S., Rossi, M., and Nucci, R. (1998) Guanidine-induced denaturation of beta-glycosidase from *Sulfolobus solfataricus* expressed in *Escherichia coli*. *Biochemistry 37*, 14484–14490.
51. Myers, J. K., Pace, C. N., and Scholtz, J. M. (1995) Denaturant m values and heat capacity changes: relation to changes in accessible surface areas of protein unfolding. *Protein Sci. 4*, 2138–2148.
52. Hubbard, S. J., and Thornton, J. M. (1993) "NACCESS" Computer Program, Department of Biochemistry and Molecular Biology, University College London.
53. Eftink, M. R. (1994) The use of fluorescence methods to monitor unfolding transitions in proteins. *Biophys. J. 66*, 482–501.
54. Ragone, R. (2000) How the protein concentration affects unfolding curves of oligomers. *Biopolymers 53*, 221–225.
55. Rose, R., Endrizzi, J., Cronk, J., Holton, J., and Alber, T. (2000) High-resolution structure of the HNF-1alpha dimerization domain. *Biochemistry 39*, 15062–15070.
56. Ibarra-Molero, B., Loladze, V. V., Makhatadze, G. I., and Sanchez-Ruiz, J. M. (1999) Thermal versus guanidine-induced unfolding of ubiquitin. An analysis in terms of the contributions from charge-charge interactions to protein stability. *Biochemistry 38*, 8138–8149.
57. Mant, C. T., Parker, J. M. R., and Hodges, R. S. (1987) Size-exclusion high-performance liquid chromatography of peptides. Requirements for peptide standards to monitor column performance and non-ideal behaviour. *J. Chromatogr. 397*, 99–112.
58. Greene, R. F., Jr., and Pace, C. N. (1974) Urea and guanidine hydrochloride denaturation of ribonuclease, lysozyme, alpha-chymotrypsin, and beta-lactoglobulin. *J. Biol. Chem. 249*, 5388–5393.
59. O'Brien, E. P., Dima, R. I., Brooks, B., and Thirumalai, D. (2007) Interactions between hydrophobic and ionic solutes in aqueous guanidinium chloride and urea solutions: lessons for protein denaturation mechanism. *J. Am. Chem. Soc. 129*, 7346–7353.
60. Li, Z., and Lazaridis, T. (2003) Thermodynamic contributions of the ordered water molecule in HIV-1 protease. *J. Am. Chem. Soc. 125*, 6636–6637.
61. Suck, D., and Ficner, R. (1996) Structure and function of PCD/DCoH, an enzyme with regulatory properties. *FEBS Lett. 389*, 35–39.
62. Ahmed, F., and Modrek, B. (1992) Biosep-SEC-S high performance size-exclusion chromatographic columns for proteins and peptides. *J. Chromatogr. 559*, 25–33.
63. Stevens, F. J. (1989) Analysis of protein-protein interaction by simulation of small-zone size exclusion chromatography. Stochastic formulation of kinetic rate contributions to observed high-performance liquid chromatography elution characteristics. *Biophys. J. 55*, 1155–1167.
64. Rodriguez-Larrea, D., Ibarra-Molero, B., and Sanchez-Ruiz, J. M. (2006) Energetic and structural consequences of desolvation/solvation barriers to protein folding/unfolding assessed from experimental unfolding rates. *Biophys. J. 91*, L48–L50.
65. Lai, Z., McCulloch, J., Lashuel, H. A., and Kelly, J. W. (1997) Guanidine hydrochloride-induced denaturation and refolding of transthyretin exhibits a marked hysteresis: equilibria with high kinetic barriers. *Biochemistry 36*, 10230–10239.
66. Mishra, R., Olofsson, L., Karlsson, M., Carlsson, U., Nicholls, I. A., and Hammarstrom, P. (2008) A conformationally isoformic thermophilic protein with high kinetic unfolding barriers. *Cell. Mol. Life Sci. 65*, 827–839.
67. Cronk, J. D., Endrizzi, J. A., and Alber, T. (1996) High-resolution structures of the bifunctional enzyme and transcriptional coactivator DCoH and its complex with a product analogue. *Protein Sci. 5*, 1963–1972.